Corresponding author: Lovro Palaversa
lp@irb.hr

Draft version November 7, 2023
Typeset using LaTeX **twocolumn** style in AASTeX631

PhotoD: LSST photometric distances out to 100 kpc.

Lovro Palaversa ,[1] Željko Ivezić ,[2] and Karlo Mrakovčić [3]

[1] *Ruđer Bošković Institute, Bijenička cesta 54, 10000 Zagreb, Croatia*
[2] *Department of Astronomy, University of Washington, Box 351580, Seattle, WA 98195, USA*
[3] *Faculty of Physics, University of Rijeka, Radmile Matejčić 2, 51000 Rijeka, Croatia*

ABSTRACT

Abstract here, mind the 250 word limit.

Keywords: Distance measure (395) — Interstellar extinction (841) — Photometry (1234) — Stellar distance (1595) — Two-color diagrams (1724)

1. INTRODUCTION

Thanks to the *Vera C. Rubin* observatory's *Legacy Survey of Space and Time* (LSST), for the first time in history, an astronomical catalog will contain more Milky Way stars than there are living people on Earth – of the order 10-20 billion, depending on model assumptions. In order to map the Milky Way in three dimensions, distances to these stars must be accurately estimated. In this paper we describe a method that will deliver LSST-based stellar distance estimations complementary to *Gaia's* state-of-the-art trigonometric parallaxes and reach about 10 times further, to approximately 100 kpc. These results will be transformative for the studies of the Milky Way in general, and the stellar and the dark matter halo in particular as never before was there a survey that simultaneously observed roughly two thirds of the sky, to the co-added depth of $r{\approx}26$ mag.

A bit about the importance of the distance estimation in the MW, dust implications (for extragalactic science too).

There are a variety of astronomical methods to estimate distances to stars, ranging from direct geometric (trigonometric) methods for nearby stars to indirect methods based on astrophysics for more distant stars.

Mention Bailer-Jones et al. (2021), Gordon et al. (2016), Green et al. (2014, 2015, 2019), Jurić et al. (2008) and Lallement et al. (2014), Queiroz et al. (2018).

Layout of the paper is...

2. METHOD

The photometric distance estimation method (hereafter `photoD`) is conceptually quite simple and relies on the strong correlations between the stellar colors and spectral energy distributions (SED) for dominant stellar populations. The SEDs, and consequently colors, are determined by the effective temperature ($T_{\rm eff}$), the surface gravity (usually denoted as $log(g)$), and the metallicity ($[M/H]$), or alternatively, by the absolute magnitude in band b ($M_{\rm b}$), $[M/H]$ and age.

The distributions that describe these correlations are obtained either from models or from observations. For example, the distribution of stellar SEDs in the color-color diagram in the middle and left panels of Figure 1 provide key insights in stellar evolution and classification of different stellar populations such as main-sequence stars, giant stars, white dwarf stars, a majority of unresolved binary stars and even extragalactic objects. Analogous distributions are responsible for the abundant structure seen in the Hertzsprung-Russell diagram (HRD).

Metallicity is an important factor in these correlations, as it has a strong effect on the luminosity of the stars. This is reflected in the width of the main stellar loci of the two-color diagrams (middle and right hand panels in Figure 1 and the color-absolute magnitude diagrams (CAMD) in Figure 2. The best photometric estimators of metallicity are colors whose shorter-wavelength component includes the metal absorbtion bands at near-UV wavelengths, short of Balmer break ($300 \lessapprox \lambda$ [nm] $\lessapprox 400$). Therefore, the LSST has a comparative advantage over the surveys lacking u-band measurements, and could provide accurate distances within the range of 5-10%. A plot of model spectra, fixed, *log(g)* and T_{eff}, several different metallicities?

Extinction is another major source of systematic errors in the process of luminosity and distance determination. The fact that the extinction vector is nearly parallel to the main stellar locus in the two-color diagrams gives rise to degeneracies that complicate the determination of the stellar type. An example is displayed in Figure 3, where in the left panel any of the different star types designated as 1,2 and 3 can have the same observed colors as the star marked as "Obs". This degeneracy is a result of the combination of colors chosen for the two-color diagram and depends on the position on the stellar locus and the adopted extinction curve parametrized by a single parameter R_V

$$R_V = \frac{A_V}{E(B-V)}, \tag{1}$$

where A_V stands for extinction in V-band and *E(B-V)* is the color excess. This relationship can be extended to an arbitrary photometric bandpass λ:

$$A_\lambda = C_\lambda(R_V) A_r, \tag{2}$$

with A_r designating extinction in r-band and $C_\lambda(R_V)$ describing the shape of the extinction curve. The degeneracy from the left panel in Figure 3 can be broken if several different colors are used, particularly those towards the infrared. There the stellar locus is not as kinked and the extinction vector is not parallel to it. A possible example is shown in the right-hand panel of the Fig. 3, where $r-i$ and $i-z$ colors are used, and assuming a fixed extinction law a unique solution for the extinction is possible.

Explain the choice of RV.

Another important degeneracy arises from the fact that even for a fixed $T_{\rm eff}$ and $[Fe/H]$, the $log(g)$ and thus the luminosity are not uniquely determined by the colors: a degeneracy may exist between the giant branch and the main sequence as the colors constructed from *ugrizy* bands are not sensitive to $log(g)$.

We adopt a Bayesian framework in which we simultaneously fit for $M_{\rm b}$, $[Fe/H]$ and $A_{\rm r}$, assuming a fixed RV value of 3.1[1] The posterior for each individual star with LSST photometry is then given as:

$$P(M_{\rm b},\, [Fe/H],\, A_{\rm r}\,|\,\vec{c}) = \frac{P(\vec{c}\,|\,M_{\rm b},\, [Fe/H],\, A_{\rm r})\, P(M_{\rm b},\, [Fe/H],\, A_{\rm r})}{P(\vec{c})} \tag{3}$$

with $\vec{c}$ standing for the vector of input colors (u-g, g-r and so on). The log-likelihood is given by:

$$ln(\mathcal{L}) = C - \frac{1}{2}\sum_{i=1}^{N}\left(\frac{c_i^{obs} - c_i^{mod}}{\sigma_i}\right)^2 \tag{4}$$

where c_i^{obs} are the observed colors and c_i^{mod} the model colors. The priors are established by partitioning the TRILEGAL galaxy model (Dal Tio et al. 2022) in healpixels, and each of the pixel in one-magnitude wide bins in apparent magnitude. The model colors are then obtained from models based on SDSS results (reference), where the input for the models are the $M_{\rm r}$ and the $[Fe/H]$ obtained from TRILEGAL. Given the assumed extinction curve, these colors are then reddened up to the maximum reddening which is estimated from Schlegel et al. (1998) (SFD98) maps. The latter upper

[1] In principle RV could be also fitted for.

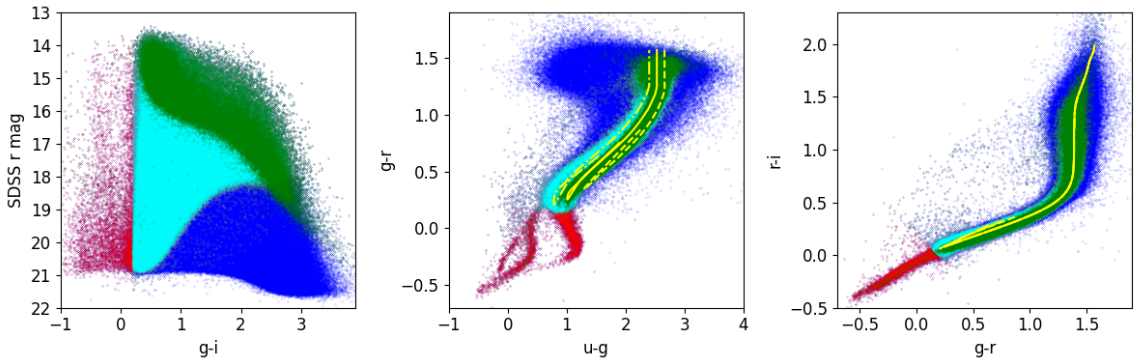

Figure 1. The blue dots in the left panel show color-magnitude diagram for 841,000 stars from the SDSS Stripe 82 Standard Star Catalog that have Gaia matches within 0.15 arcsec (after correcting for proper motion using Gaia measurements). A subset of 415,000 stars with $r < 22$ and $u < 22$ are shown as red dots, and 409,000 of those that also have $0.2 < g - i < 3.5$ are shown as cyan dots. Finally, 63,000 stars that have signal-to-noise ratio for Gaia's parallax measurements of at least 20 are shown as green dots. The same color scheme is used in other two panels. The three yellow lines in the middle panel show stellar locus parametrization used by Green et al. (2014) for three values of metallicity (left to right): $[Fe/H] = -2.0, -1.0, 0.0$. In the right panel, the impact of metallicity on color-color tracks is negligible and all three are indistinguishable from each other.

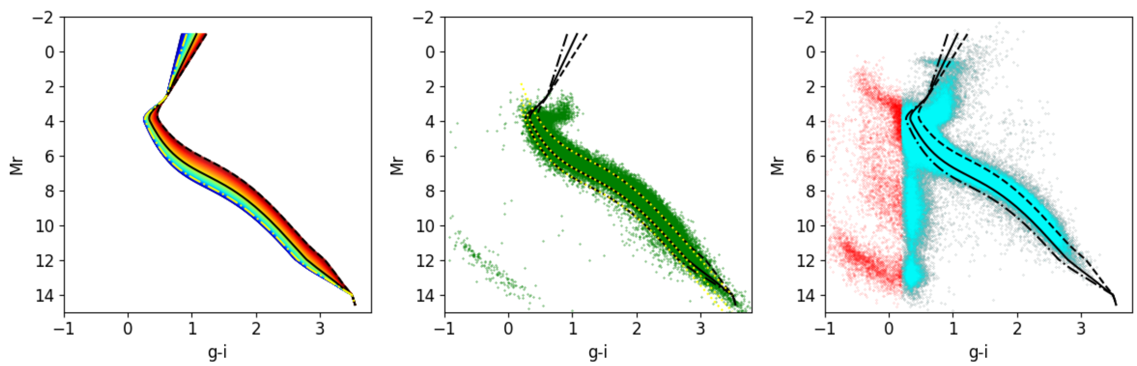

Figure 2. The left panel shows the absolute magnitude vs. color parametrization for main sequence and red giant stars. The symbols are color-coded by metallicity, ranging from $[Fe/H] = -2.5$ to 0.0 (blue to red). The three lines correspond to three values of metallicity: $[Fe/H] = -2.0, -1.0, 0.0$ (dot-dashed, solid and dashed, respectively). The middle panel shows a sample of 63,000 stars that have signal-to-noise ratio for Gaia's parallax measurements of at least 20 (white dwarfs can be seen in the lower left corner). The dot-dashed, solid and dashed black lines are the same as in the left panel. For comparison, the dotted lines were computed using eqs. A2 and A7 from Ivezic et al. (2008). The right panel shows a sample of 415,000 stars with $r < 22$ and $u < 22$ as red dots, and 409,000 of those that also have $0.2 < g - i < 3.5$ as cyan dots. Their absolute magnitudes were computed using the so-called "photo-geometric" distances from Bailer-Jones et al. (2021). The dot-dashed, solid and dashed black lines are the same as in the left and middle panels. About 10,000 outliers seen at $g - i = 0.4$ and $Mr > 7$ are predominantly found at the faint end ($r > 20$).

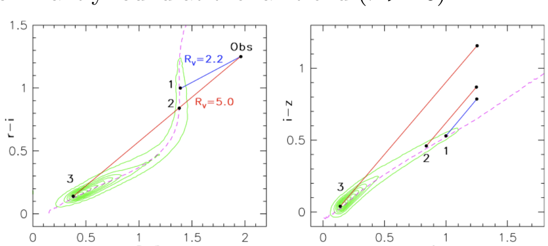

Figure 3. Add caption.

limit is used in order to provide a realistic stop condition on the amount of extinction and reduce the processing time. This is usually a valid assumption because the SFD98 maps provide *total* extinction along a line of sight. In order to account for the eventual underestimation in the SFD98 maps we increase the SFD98 extinctions by 20%.

Our fitting procedure is also executed on an adaptive grid, a coarse search over the parameter space is performed first in order to establish the layout of the manifold. However, care is taken that any possible local minima are not missed by appropriately adjusting the step size how?. The located maxima are then explored with a smaller step size (adjusted how?).

In addition to the approach described here, we also tested Markov Chain Monte Carlo and neural network approaches that will be/are described in forthcoming/published papers.

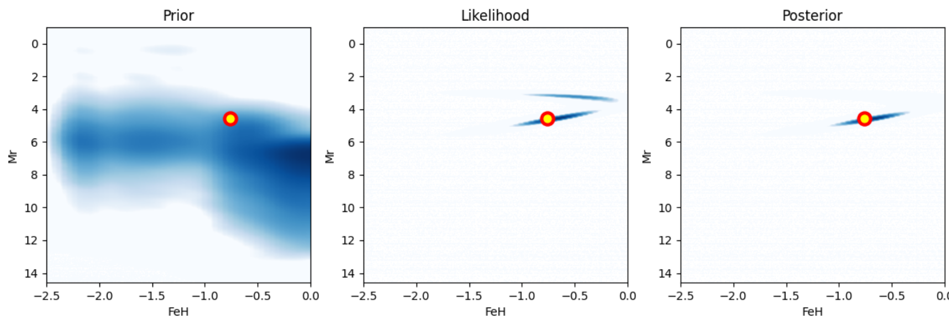

Figure 4. Write caption: prior, likelihood, posterior maps

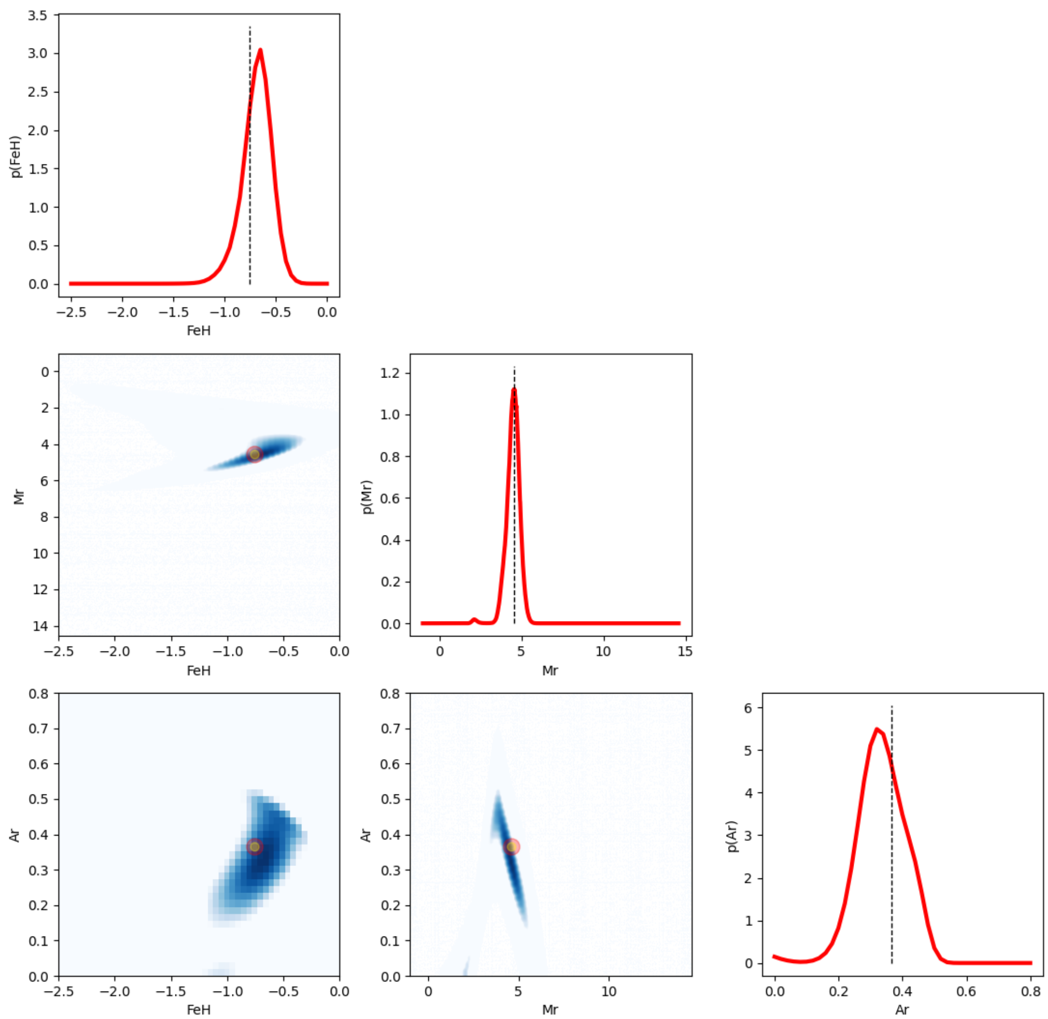

Figure 5. Write caption: 2-param covariances and marginal distributions

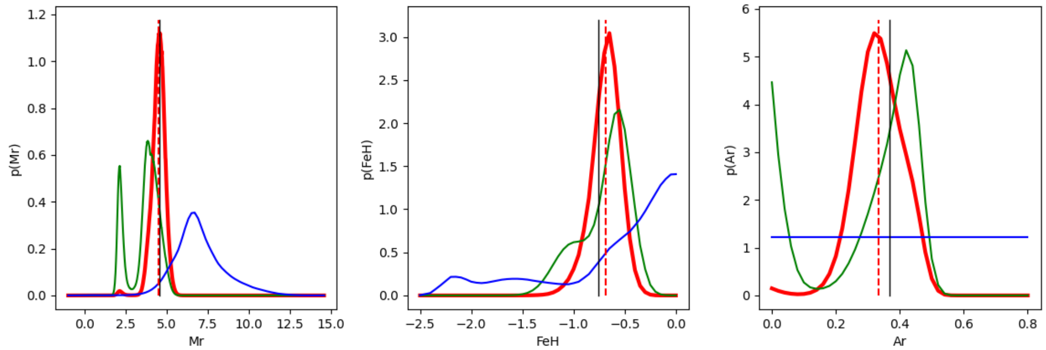

Figure 6. Write caption: prior, likelihood, posterior marginal distributions

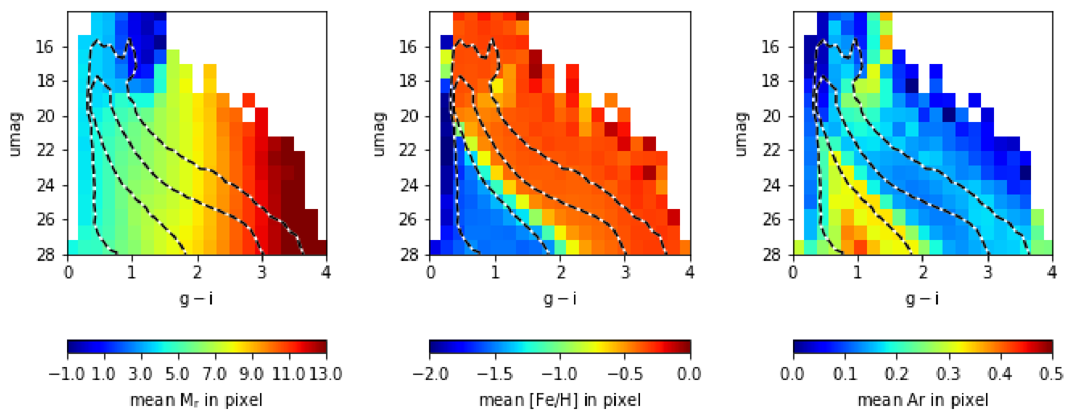

Figure 7. Write caption: TRILEGAL mean values of input model params in umag vs. g-i

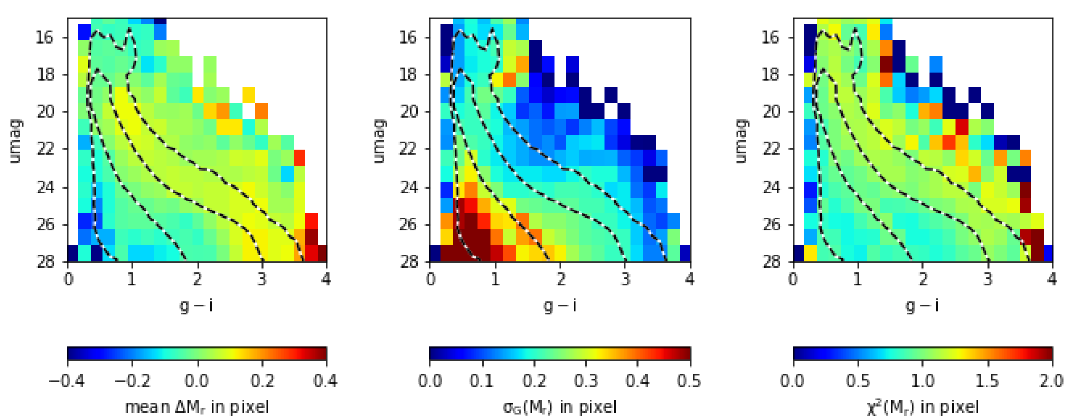

Figure 8. Write caption: performance for Mr vs. true Mr and FeH

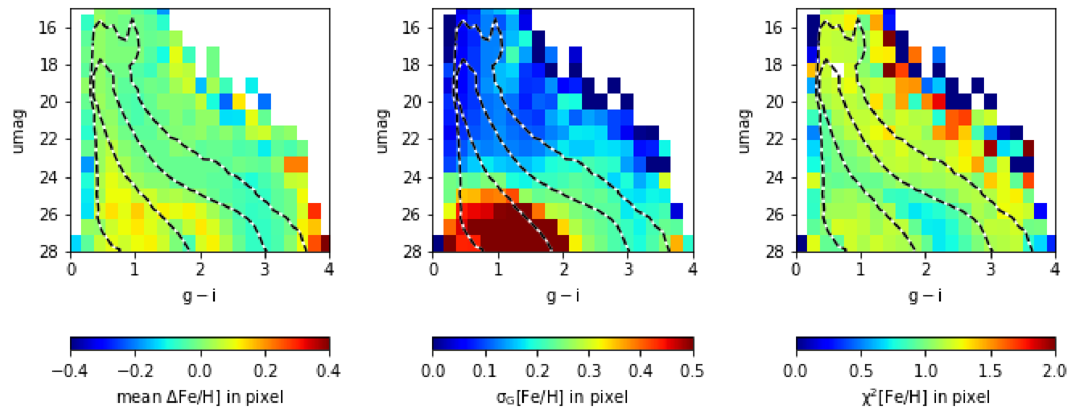

Figure 9. Write caption: performance for FeH vs. true Mr and FeH

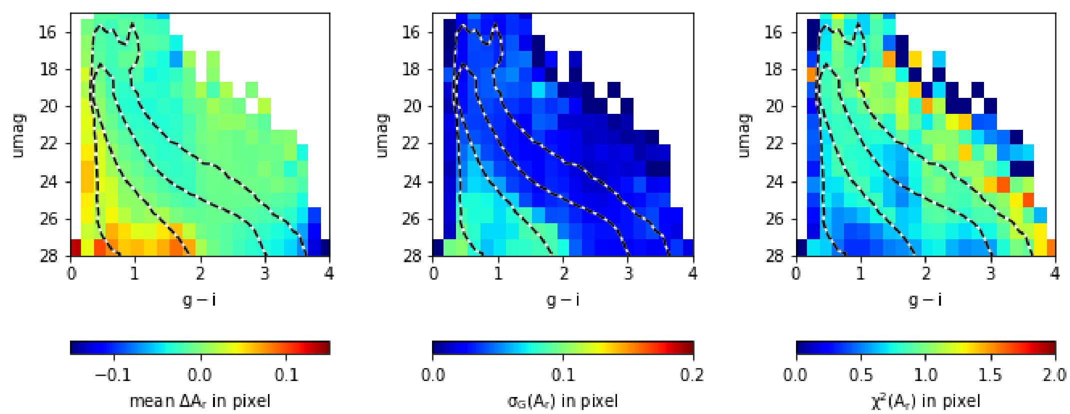

Figure 10. Write caption: performance for Ar vs. true Mr and FeH

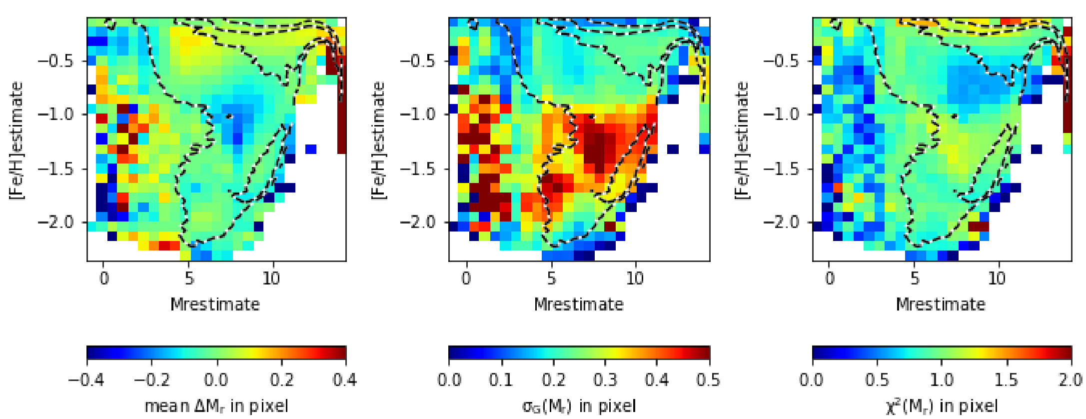

Figure 11. Write caption: performance for Mr vs. estimated Mr and FeH

APPENDIX

REFERENCES

Bailer-Jones, C. A. L., Rybizki, J., Fouesneau, M., Demleitner, M., & Andrae, R. 2021, AJ, 161, 147, doi: 10.3847/1538-3881/abd806

Dal Tio, P., Pastorelli, G., Mazzi, A., et al. 2022, The Astrophysical Journal Supplement Series, 262, 22, doi: 10.3847/1538-4365/ac7be6

Gordon, K. D., Fouesneau, M., Arab, H., et al. 2016, The Astrophysical Journal, 826, 104, doi: 10.3847/0004-637X/826/2/104

Green, G. M., Schlafly, E., Zucker, C., Speagle, J. S., & Finkbeiner, D. 2019, The Astrophysical Journal, 887, 93, doi: 10.3847/1538-4357/ab5362

Green, G. M., Schlafly, E. F., Finkbeiner, D. P., et al. 2014, ApJ, 783, 114, doi: 10.1088/0004-637X/783/2/114

—. 2015, ApJ, 810, 25, doi: 10.1088/0004-637X/810/1/25

Jurić, M., Ivezić, Ž., Brooks, A., et al. 2008, The Astrophysical Journal, 673, 864, doi: 10.1086/523619

Lallement, R., Vergely, J.-L., Valette, B., et al. 2014, A&A, 561, A91, doi: 10.1051/0004-6361/201322032

Queiroz, A. B. A., Anders, F., Santiago, B. X., et al. 2018, Monthly Notices of the Royal Astronomical Society, 476, 2556, doi: 10.1093/mnras/sty330

Schlegel, D. J., Finkbeiner, D. P., & Davis, M. 1998, The Astrophysical Journal, 500, 525, doi: 10.1086/305772